Human Visual System-Based Image Enhancement and Logarithmic Contrast Measure

Karen A. Panetta, *Fellow, IEEE*, Eric J. Wharton, *Student Member, IEEE*, and Sos S. Agaian, *Senior Member, IEEE*

***Abstract*—Varying scene illumination poses many challenging problems for machine vision systems. One such issue is developing global enhancement methods that work effectively across the varying illumination. In this paper, we introduce two novel image enhancement algorithms: edge-preserving contrast enhancement, which is able to better preserve edge details while enhancing contrast in images with varying illumination, and a novel multihistogram equalization method which utilizes the human visual system (HVS) to segment the image, allowing a fast and efficient correction of nonuniform illumination. We then extend this HVS-based multihistogram equalization approach to create a general enhancement method that can utilize any combination of enhancement algorithms for an improved performance. Additionally, we propose new quantitative measures of image enhancement, called the logarithmic Michelson contrast measure (AME) and the logarithmic AME by entropy. Many image enhancement methods require selection of operating parameters, which are typically chosen using subjective methods, but these new measures allow for automated selection. We present experimental results for these methods and make a comparison against other leading algorithms.**

***Index Terms*—Enhancement measure, human visual system (HVS), image enhancement, logarithmic image processing.**

I. Introduction

PROVIDING digital images with good contrast and detail is required for many important areas such as vision, remote sensing, dynamic scene analysis, autonomous navigation, and biomedical image analysis [3]. Producing visually natural images or modifying an image to better show the visual information contained within the image is a requirement for nearly all vision and image processing methods [9]. Methods for obtaining such images from lower quality images are called image enhancement techniques. Much effort has been spent in extracting information from properly enhanced images [1], [2], [4]–[8]. The enhancement task, however, is complicated by the lack of any general unifying theory of image enhancement as well as the lack of an effective quantitative standard of image quality to act as a design criterion for an image enhancement system.

Furthermore, many enhancement algorithms have external parameters which are sometimes difficult to fine-tune [11]. Most of these techniques are globally dependent on the type of input and treat images instead of adapting to local features within different regions [12]. A successful automatic image enhancement requires an objective criterion for enhancement and an external evaluation of quality [9].

Recently, several models of the human visual system (HVS) have been used for image enhancement. One method is to attempt to model the transfer functions of the parts of the HVS, such as the optical nerve, cortex, and so forth. This method then attempts to implement filters which recreate these processes to model human vision [41], [42]. Another method uses a single channel to model the entire system, processing the image with a global algorithm [42].

HVS-based image enhancement aims to emulate the way in which the HVS discriminates between useful and useless data [34]. Weber's Contrast Law quantifies the minimum change required for the HVS to perceive contrast; however, this only holds for a properly illuminated area. The minimum change required is a function of background illumination and can be closely approximated with three regions. The first is the Devries–Rose region, which approximates this threshold for under-illuminated areas. The second and most well known region is the Weber region, which models this threshold for properly illuminated areas. Finally, there is the saturation region, which approximates the threshold for over-illuminated areas [33]. Each of these regions can be separately enhanced and recombined to form a more visually pleasing output image.

In this paper, we propose a solution to these image enhancement problems. The HVS system of image enhancement first utilizes a method which segments the image into three regions with similar qualities, allowing enhancement methods to be adapted to the local features. This segmentation is based upon models of the HVS.

The HVS system uses an objective evaluation measure for selection of parameters. This allows for more consistent results while reducing the time required for the enhancement process. The performance measure utilizes established methods of measuring contrast and processes these values to assess the useful information contained in the image. Operating parameters are selected by performing the enhancement with all practical values of the parameters, by assessing each output image using the measure, and by organizing these results into a graph of performance measure versus parameters, where the best parameters are located at local extrema.

Manuscript received February 26, 2007; revised June 8, 2007. This work was supported in part by the National Science Foundation under Award 0306464. This paper was recommended by Associate Editor P. Bhattacharya.

K. A. Panetta and E. J. Wharton are with the Department of Electrical and Computer Engineering, Tufts University, Medford, MA 02155 USA (e-mail: karen@eecs.tufts.edu; ewhart02@eecs.tufts.edu).

S. S. Agaian is with the College of Engineering, University of Texas at San Antonio, San Antonio, TX 78249 USA, and also with the Department of Electrical and Computer Engineering, Tufts University, Medford, MA 02155 USA (e-mail: sos.agaian@utsa.edu).

Color versions of one or more of the figures in this paper are available online at http://ieeexplore.ieee.org.

Digital Object Identifier 10.1109/TSMCB.2007.909440

This paper is organized as follows. Section II presents the necessary background information, including the parameterized logarithmic image processing (PLIP) model operator primitives, used to achieve a better image enhancement, several enhancement algorithms, including modified alpha rooting and logarithmic enhancement, and the multiscale center-surround Retinex algorithm, which we use for comparison purposes. Section III presents new contrast measures, such as the logarithmic Michelson contrast measure (AME) and logarithmic AME by entropy (AMEE), and a comparison with other measures used in practice, such as the measure of image enhancement (EME) and AME. Section IV introduces the new HVS-based segmentation algorithms, including HVS-based multihistogram equalization and HVS-based image enhancement. Section V discusses in detail several new enhancement algorithms, including edge-preserving contrast enhancement (EPCE) and the logarithm and AME-based weighted passband (LAW) algorithm. Section VI presents a computational analysis comparing the HVS algorithm to several state-of-the-art image enhancement algorithms, such as low curvature image simplifier (LCIS). Section VII presents the results of computer simulations and analysis, comparing the HVS algorithm to Retinex and other algorithms, showing that the HVS algorithm outperforms the other algorithms. Section VIII discusses results and provides some concluding comments.

II. Background

In this section, the PLIP model, as well as several traditional algorithms which will be used with the HVS-based image enhancement model, is discussed. These algorithms include modified alpha rooting and logarithmic enhancement [32], [38], [39].

A. PLIP Model and Arithmetic

It has been shown that there are five fundamental requirements for an image processing framework. First, it must be based on a physically and/or psychophysically relevant image-formation model. Second, its mathematical structures and operations must be both powerful and consistent with the physical nature of the images. Third, its operations must be computationally effective. Fourth, it must be practically fruitful. Finally, it must not damage either signal [13], [43].

An image representation on a computer must follow some model that is physically consistent with a real-world image, whether it is a photo, object, or scene [14]. Furthermore, the arithmetic must be consistent with some real-world phenomenon, and it has been shown and is also intuitive that the HVS should be considered when developing this model [15]. It is important to consider which operations are to be used and why, and that these effectively model and are physically consistent with a real-world model for image processing [44], [45]. It must also be shown that not only the image processing model is mathematically well defined but also it must serve some useful purpose. Finally, when a visually "good" image is added to another visually "good" image, the resulting image must also be "good" [43].

The PLIP model was introduced by Panetta *et al.* [43] to provide a nonlinear framework for image processing, which addresses these five requirements. It is designed to both maintain the pixel values inside the range $(0,M]$ and more accurately process images from an HVS point of view. To accomplish this, images are processed as absorption filters using the gray tone function. This gray tone function is as follows:

$$g(i,j) = M - f(i,j) \tag{1}$$

where $f(i,j)$ is the original image function, $g(i,j)$ is the output gray tone function, and M is the maximum value of the range. It can be seen that this gray tone function is much like a photo negative.

The PLIP model operator primitives can be summarized as follows:

$$a \oplus b = a + b - \frac{ab}{\gamma(M)} \tag{2}$$

$$a \Theta b = k(M)\frac{a-b}{k(M)-b} \tag{3}$$

$$c \otimes a = \gamma(M) - \gamma(M)\left(1 - \frac{a}{\gamma(M)}\right)^{c} \tag{4}$$

$$a * b = \varphi^{-1}\left(\varphi(a)\cdot\varphi(b)\right) \tag{5}$$

$$\varphi(a) = -\lambda(M)\cdot \ln^{\beta}\left(1 - \frac{f}{\lambda(M)}\right) \tag{6}$$

$$\varphi^{-1}(a) = -\lambda(M)\cdot\left[1 - \exp\left(\frac{-f}{\lambda(M)}\right)^{1/\beta}\right] \tag{7}$$

where we use $\oplus$ as PLIP addition, Θ as PLIP subtraction, $\otimes$ as PLIP multiplication by a scalar, and $*$ as PLIP multiplication of two images. Also, a and b are any gray tone pixel values, c is a constant, M is the maximum value of the range, and β is a constant. $\gamma(M)$, $k(M)$, and $\lambda(M)$ are all arbitrary functions. We use the linear case, such that they are functions of the type $\gamma(M) = AM + B$, where A and B are integers; however, any arbitrary function will work. In general, a and b correspond to the same pixel in two different images that are being added, subtracted, or multiplied. In [43], the best values of A and B were experimentally determined to be any combination such that $\gamma(M)$, $k(M)$, and $\lambda(M) = 1026$, and the best value of β was determined to be $\beta = 2$.

B. Alpha Rooting and Logarithmic Enhancement

Alpha rooting is a straightforward method originally proposed by Jain [54]. This enhancement algorithm was later modified by Aghagolzadeh and Ersoy [40], as well as by Agaian *et al.* [38], [39]. Alpha rooting is an algorithm that can be used in combination with many different orthogonal transforms such as the Fourier, Hartley, Haar wavelet, and cosine transforms. The resulting output shows an emphasis on the high-frequency content of the image without changing the phase of the transform coefficients, resulting in an overall contrast enhancement. This enhancement, however, can sometimes result in ugly artifacts [37].

Alpha rooting and logarithmic enhancement are transform-based enhancement methods [32]. This means that they first

perform some 2-D orthogonal transform on the input image and then modify these transform coefficients. Alpha rooting modifies the coefficients according to the following formula:

$$O(p,s) = X(p,s) \times |X(p,s)|^{\alpha-1} \tag{8}$$

where $X(p,s)$ is the 2-D Fourier transform of the input image, $O(p,s)$ is the 2-D Fourier transform of the output image, and α is a user-defined operating parameter with range $0 < \alpha < 1$.

Logarithmic enhancement was introduced by Agaian in [32], [38], and [39]. This method also reduces the transform coefficient magnitudes while leaving the phase unchanged, using a logarithmic rule. Logarithmic enhancement uses two parameters, namely, β and λ. It works according to the following transfer function:

$$O(p,s) = \log^{\beta}\left(|X(p,s)|^{\lambda} + 1\right). \tag{9}$$

C. Multiscale Center-Surround Retinex

The multiscale center-surround Retinex algorithm was developed by Jobson *et al.* [36]. This algorithm was developed to attain lightness and color constancy for machine vision applications. While there is no single complete definition for the Retinex model, lightness and color constancy refer to the resilience of perceived color and lightness to spatial and spectral illumination variations. Benefits of the Retinex algorithm include dynamic range compression and color independence from the special distribution of the scene illumination. However, this algorithm can result in "halo" artifacts, especially in boundaries between large uniform regions. Also, a "graying out" can occur, in which the scene tends to change to middle gray.

The Retinex algorithm works by processing the image with a high-pass filter, using several different widths and averaging the results together. The algorithm is executed as follows:

$$R(i,j) = \sum_{n=1}^{N} w_n \log\left(I(i,j)\right) - \log\left(F(i,j) * I(i,j)\right) \tag{10}$$

where $I(i,j)$ is the input image, $R(i,j)$ is the output image, $F(i,j)$ is a Gaussian kernel normalized to sum to one, w_n is a collection of weights, and $*$ for this algorithm is the convolution operator. In general, the weights w_n are chosen to be equal. This is a particular case of the Retinex algorithm.

III. Contrast Measure and Properties

An important step in a direct image enhancement approach is to create a suitable performance measure. The improvement found in the resulting images after enhancement is often very difficult to measure. This problem becomes more apparent when the enhancement algorithms are parametric, and one needs to choose the best parameters, to choose the best transform among a class of unitary transforms, or to automate the image enhancement procedures. The problem becomes especially difficult when an image enhancement procedure is used as a preprocessing step for other image processing purposes such as object detection, classification, and recognition.

There is no universal measure which can specify both the objective and subjective validity of the enhancement method [22]. However, in [16], the three necessary characteristics of a performance measure are given. First, it must measure the desired characteristic in some holistic way. In our case, this is contrast. Second, it must show a proportional relationship between increase and decrease of this characteristic. Finally, it must have some resulting characteristic to find optimal points. One example of this is using local extrema. In this section, we analyze the commonly used performance measures and present two new quantitative contrast measures, called the logarithmic AME and logarithmic AMEE, to address these three characteristics. Since we are measuring improvement in enhancement based on contrast, we will use enhancement and contrast measures interchangeably.

A. New Contrast Measure

Many enhancement techniques are based on enhancing the contrast of an image [17]–[20]. There have been many differing definitions of an adequate measure of performance based on contrast [21]–[23]. Gordon and Rangayan used local contrast defined by the mean gray values in two rectangular windows centered on a current pixel. Beghdadi and Negrate [21] defined an improved version of the aforementioned measure by basing their method on a local edge information of the image. In the past, attempts at statistical measures of gray level distribution of local contrast enhancement such as those based on mean, variance, or entropy have not been particularly useful or meaningful. A number of images, which show an obvious contrast improvement, showed no consistency, as a class, when using these statistical measurements. Morrow *et al.* [23] introduced a measure based on the contrast histogram, which has a much greater consistency than statistical measures.

Measures of enhancement based on the HVS have been previously proposed [24]. Algorithms based on the HVS are fundamental in computer vision [25]. Two definitions of contrast measure have traditionally been used for simple patterns [26]: Michelson [27], [28], which is used for periodic patterns like sinusoidal gratings, and Weber, which is used for large uniform luminance backgrounds with small test targets [26]. However, these measures are not effective when applied to more difficult scenarios such as images with nonuniform lighting or shadows [26], [35]. The first practical use of a Weber's-law-based contrast measure, the image enhancement measure or contrast measure, was developed by Agaian [30].

This contrast measure was later developed into the EME, or measure of enhancement, and the EMEE, or measure of enhancement by entropy [29], [31]. Finally, the Michelson Contrast Law was included to further improve the measures. These were called the AME and AMEE [16]. These are summarized in [16] and are calculated by dividing an image into $k1 \times k2$ blocks, by calculating the measure for each block, and by averaging the results as shown in the formula definitions.

In this paper, we capitalize on the strengths of these measures and improve upon them by including the PLIP operator

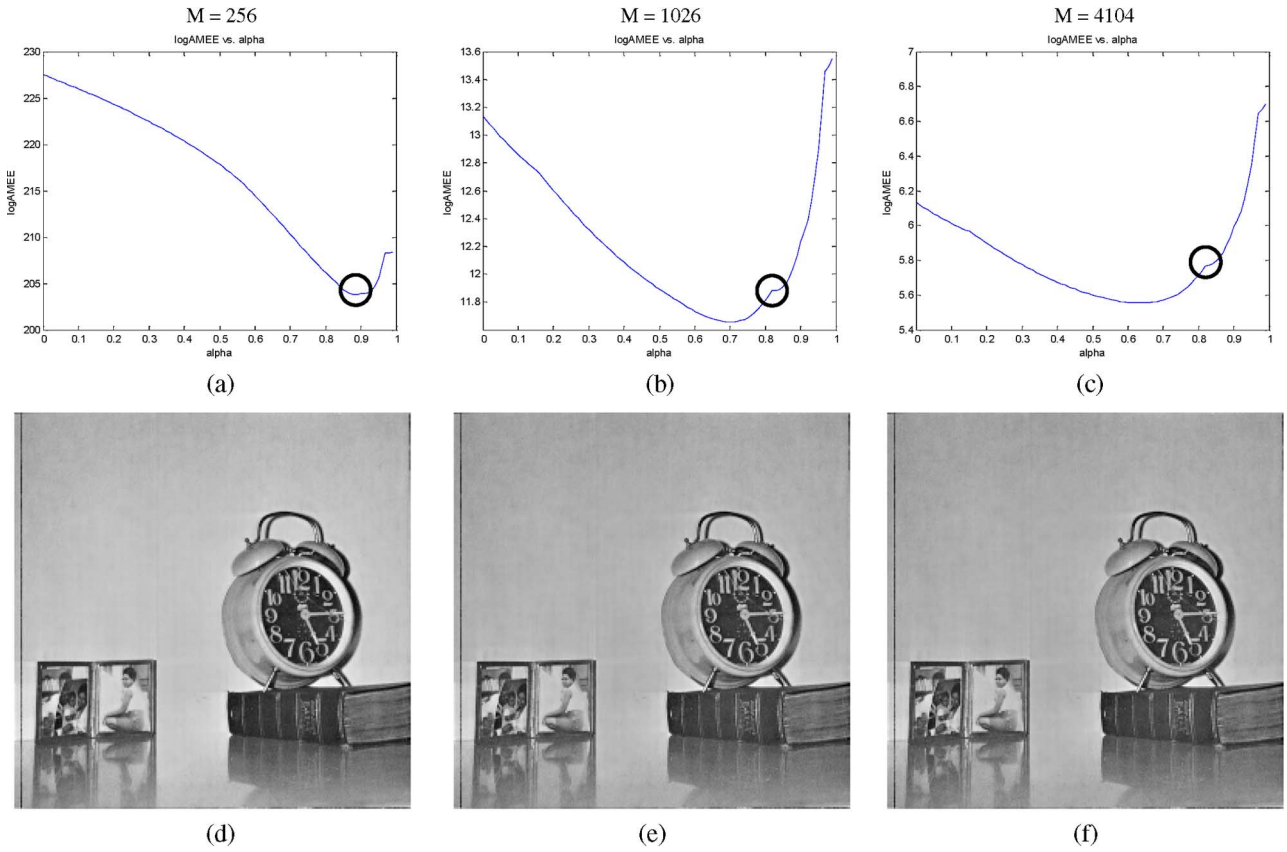

Fig. 1. Optimizing the logarithmic AMEE measure as given in (12) by choosing the best value for M. (a)–(c) Logarithmic AMEE graphs using $M = 256$, $M = 1026$, and $M = 4104$, respectively. (d)–(f) Resulting images for alpha rooting using parameters from these graphs.

primitives. This allows for a more accurate processing of the contrast information, as PLIP subtraction has been shown to be consistent with Weber's Contrast Law [13]. With these modifications, we introduce the new logarithmic AME and logarithmic AMEE measures, which are better able to assess images and thus more accurately select parameters. These new measures are presented in the following:

$$\log \mathrm{AME}_{k_1 k_2}(\Phi) = \frac{1}{k_1 k_2} \otimes \sum_{i=1}^{k_1} \sum_{j=1}^{k_2} \frac{1}{20} \otimes \ln\left(\frac{I^w_{\max:k,l} \Theta I^w_{\min:k,l}}{I^w_{\max:k,l} \oplus I^w_{\min:k,l}}\right) \tag{11}$$

$$\log \mathrm{AMEE}_{k_1 k_2}(\Phi) = \frac{1}{k_1 k_2} \otimes \sum_{i=1}^{k_1} \sum_{j=1}^{k_2} \frac{I^w_{\max:k,l} \Theta I^w_{\min:k,l}}{I^w_{\max:k,l} \oplus I^w_{\min:k,l}} * \ln\left(\frac{I^w_{\max:k,l} \Theta I^w_{\min:k,l}}{I^w_{\max:k,l} \oplus I^w_{\min:k,l}}\right). \tag{12}$$

To use the measures for selection of parameters, the algorithm is first run for all practical values of the parameters. The measure is calculated for each output image, and these data are organized into a graph as measure versus parameters. Finally, the best parameters are located at the local extrema.

B. Optimizing the PLIP for Contrast Measures

In [43], the PLIP model was optimized for image enhancement procedures. However, for purposes of image enhancement measures, these optimal values may be different. To address this, an experiment was performed using a number of different values for $\gamma(M)$, $k(M)$, and $\lambda(M)$, as given in (2)–(7), using the measures to select parameters for enhancement algorithms. In this section, we present representative results of this experiment to determine the optimal values of $\gamma(M)$, $k(M)$, and $\lambda(M)$.

Fig. 1 shows the results for the clock image using alpha rooting. Fig. 1(a) shows the logarithmic AMEE graph using $M = 256$, Fig. 1(b) shows the graph using $M = 1026$, and Fig. 1(c) shows the graph for $M = 4104$, which is another consistent value found in [43]. All of these graphs clearly satisfy the three requirements stated earlier and are easy to read. For all three graphs, the best value is located at a small peak near the absolute minimum. This peak is most obvious in the graph with $M = 1026$, occurring at $\alpha = 0.82$. For the graph with $M = 256$, this peak is located at $\alpha = 0.90$, and for the graph with $M = 4104$, this peak is located at $\alpha = 0.82$. The images with $\alpha = 0.82$ are more visually pleasing, with better contrast and definition. However, as M increases beyond 1026, the curve smooths out, which can be seen in the graph with $M = 4104$, until the peak is lost as M becomes sufficiently large. This demonstrates that $M = 1026$ is the best value for the contrast measures.

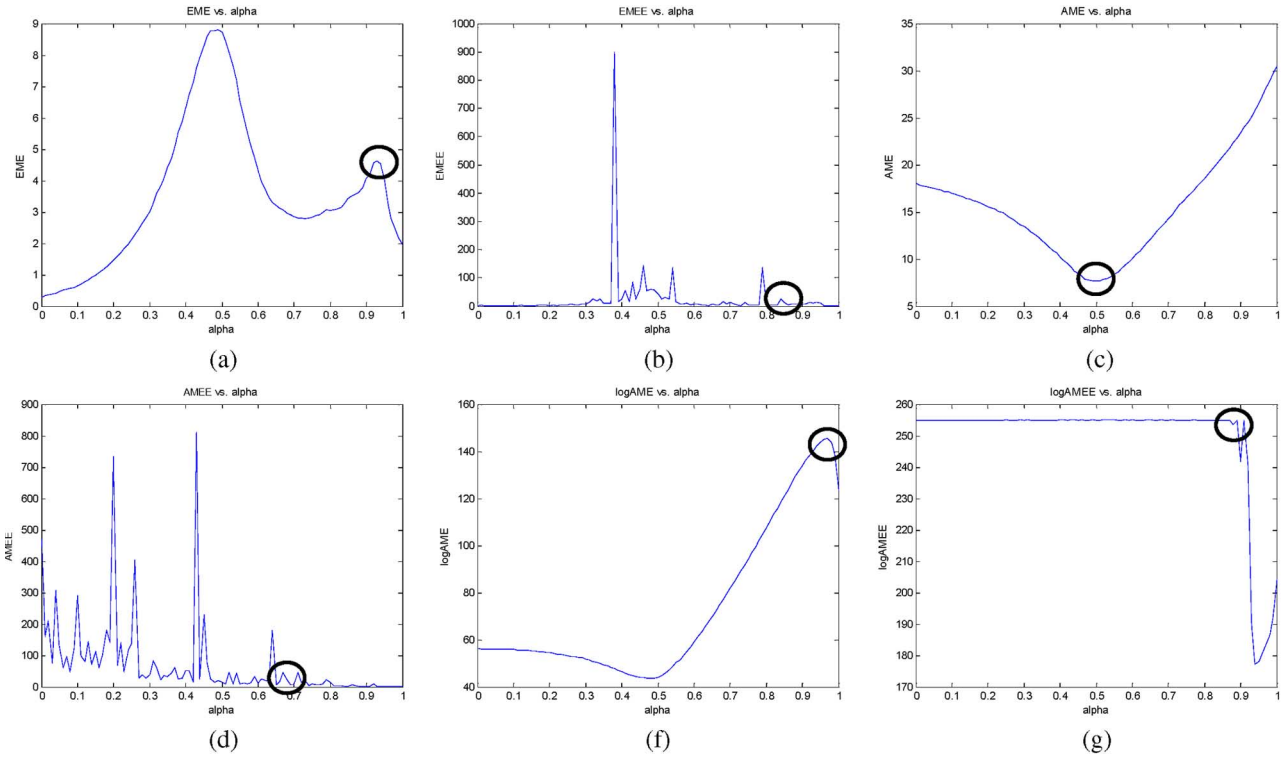

Fig. 2. Choosing the best measure for the clock image. (a) EME, (b) EMEE, (c) AME, (d) AMEE, (e) logAME, and (f) logAMEE versus alpha graphs for the clock using alpha rooting. (a), (c), (e), and (f) are the easiest to read, having only a few well-defined extrema to investigate for optimal enhancement parameter alpha.

C. Selecting the Best Measure

In this section, we use the aforementioned enhancement algorithms to select the best measure, which results in the most visually pleasing image enhancement. While it is emphasized in [16] that performance of a measure is algorithm dependent and different measures will work best with different enhancement algorithms, it is still possible to select which is best for the general case. The algorithms have been performed for numerous images using the measures presented in Section III to select parameters. We visually compared the output images to determine which measure is able to select the best parameters. For this section, we show the results of alpha rooting and logarithmic enhancement. We then present a summary for a number of algorithms.

Figs. 2 and 3 show the process of selecting parameters using the measures. Fig. 2 shows the resulting graphs generated by processing the clock image with alpha rooting, plotting the results of the measure against the values of α. Values are selected as shown, which correspond to the local extrema in the graphs. Fig. 3 shows the output images using the parameters selected from these graphs.

As the graphs in Fig. 2 show, the output form of the PLIP-based measures is smoother than the results of the measures which utilize classical arithmetic. The logarithmic AMEE, shown in Fig. 2(f), has only three local extrema. The EMEE and AMEE graphs, shown in Fig. 2(b) and (d), have many peaks. This makes the LogAMEE graph faster and easier to interpret, as there are only three values to investigate. Also, as shown in Fig. 3, the enhanced image using this value is visually more pleasing than the others. It has the best balance of sharpness and contrast, and there are no artifacts introduced.

Table I summarizes the results of this paper for all algorithms used. It shows the averaged subjective evaluations of a number of human interpreters. The algorithms were performed using all six measures to select parameters, and the evaluators were shown only the output images and were asked to rank them between 1 and 1, with 4 being the best performance and 1 being the lowest performance. The subjective evaluations show that the new PLIP-based logarithmic AME and logarithmic AMEE outperform the previously used measures.

IV. HVS-Based Segmentation

In this section, we propose a segmentation method based upon the HVS. Several models of the HVS have been introduced. One method attempts to model the transfer functions of the parts of the HVS, such as the optical nerve, cortex, and so forth. This method then attempts to implement filters which recreate these processes to model human vision [41], [42]. Another method uses a single channel to model the entire system, processing the image with a global algorithm [42].

In [51], the authors use knowledge of the HVS to segment an image into a number of subimages, each containing similar 1-D edge information. This is performed using a collection of known 1-D curves. They show that, along with the gradient information along those curves, this is a complete representation of the image. We expand upon this by segmenting an image into a collection of 2-D images, all with similar internal properties.

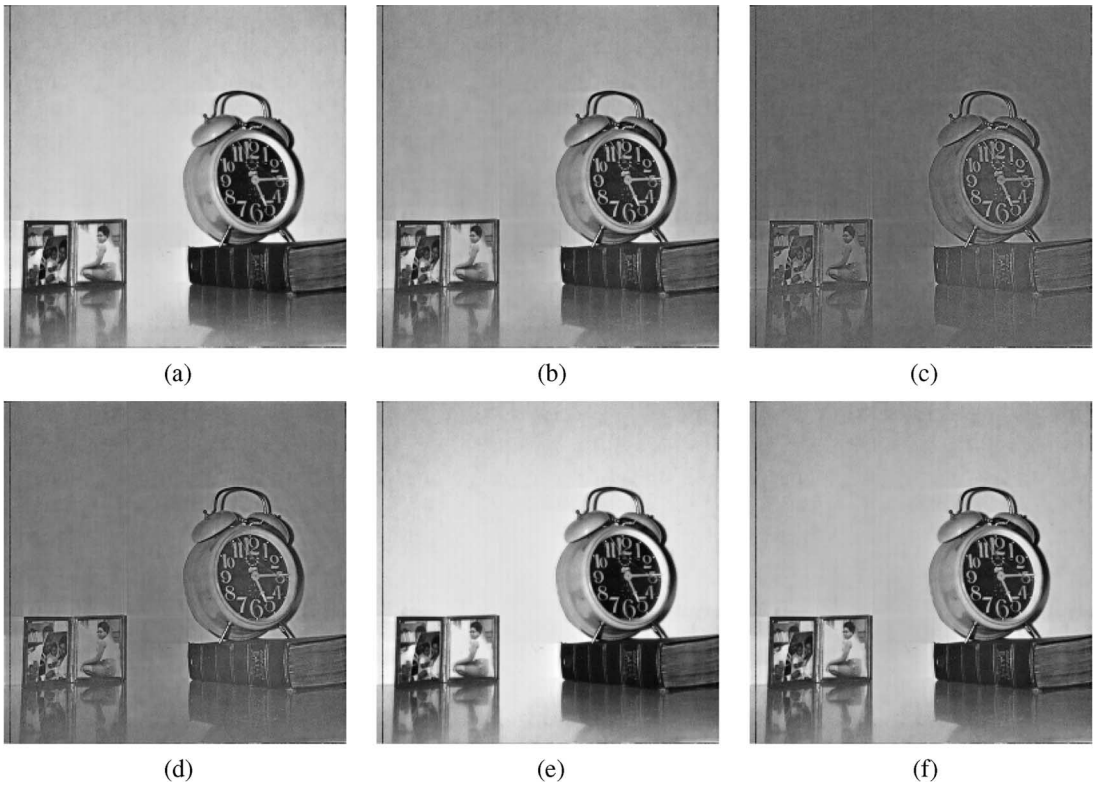

Fig. 3. Output images of the clock using alpha rooting, with parameters selected using (a) EME, (b) EMEE, (c) AME, (d) AMEE, (e) logAME, and (f) logAMEE. (a), (b), and (f) are the best results, with good sharpness and contrast, as (f) comes from the easiest to read graph. LogAMEE is best for this image and enhancement algorithm.

TABLE I
COMPARISON OF MEASURES BY PERFORMANCE

Algorithm	EME	EMEE	AME	AMEE	logAME	logAMEE
Bi-Histogram Equalization	**	***	**	**	****	***
Alpha Rooting	**	***	*	**	**	****
NLE	**	**	*	*	***	****
Logarithmic Enhancement	*	*	**	**	***	****
* = Low Performance, ** = Fair, *** = Good, **** = Best						

However, to perform the 2-D segmentation, we also use the gradient information, but this is not sufficient. We also need to know background illumination.

In this paper, we present a new application of the HVS. The HVS-based image enhancement model segments an image based upon background intensity and gradient. The minimum gradient required for the HVS to detect a change is a function of background illumination and can be closely approximated with three regions, as shown in Fig. 4. These are the Devries–Rose region, for under-illuminated areas; the Weber region, for properly illuminated areas; and the saturation region, which approximates the threshold for over-illuminated areas. There is also a fourth region that consists of all the pixels underneath the curve [33], [52], [53].

By using this model, we have an automated method for segmenting an image into these three regions. As these regions individually have uniform illumination, traditional histogram equalization can be applied to effectively correct these issues and enhance the image. This process is further improved by calculating the threshold for each region, by discarding those pixels which do not constitute a noticeable contrast, and by categorizing these pixels into region 4. In this manner, less meaningful pixels are removed from the enhancement process, reducing artifacts. In the succeeding discussions, we present a new method of calculating these thresholds.

HVS image enhancement performs this segmentation using the background intensity and the rate of change information. The background intensity is calculated as a weighted local mean, and the rate of change is calculated as a gradient measurement. The background intensity is derived by using the following formula, where $B(x,y)$ is the background intensity at each pixel, $X(x,y)$ is the input image, Q is all of the pixels which are directly up, down, left, and right from the pixel, Q' is all of the pixels diagonally one pixel away, and l and q are some constant:

$$B(x,y) = l \otimes \left[l \otimes \left(\frac{l}{2} \otimes \sum_{Q} X(i,j) \oplus \frac{q}{2} \otimes \sum_{Q'} X(k,l) \right) \oplus X(x,y) \right]. \quad (13)$$

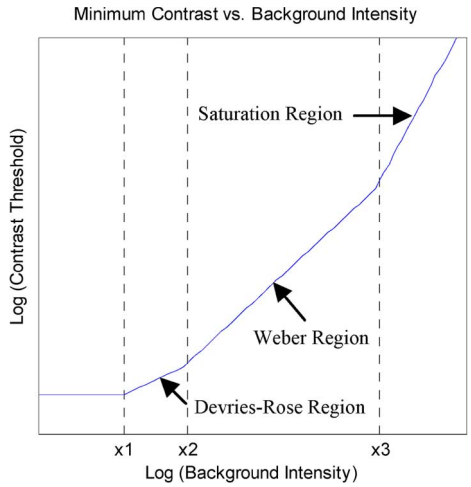

Fig. 4. Four regions of human visual response. Devries–Rose from x_1 to x_2, Weber from x_2 to x_3, saturation from x_3 to infinity, and the fourth region below the line, containing the least informative pixels.

We must also define a parameter B_T, which is the maximum difference in the image, derived by using

$$B_T = \max\left(X(x,y)\right) \ominus \min\left(X(x,y)\right). \tag{14}$$

Furthermore, the gradient information is needed, which is derived by using any of the edge-detection methods. We will define $X'(x,y)$ as the result of this operation. Finally, we must also know some thresholding parameters concerning the human eye itself, which we will call B_{xi}, $i = 1,2,3$ for the background illumination thresholds and K_i, $i = 1,2,3$ for the gradient thresholds. These are obtained using the following formulas, where α_1, α_2, and α_3 are parameters based upon the three different regions of response characteristics displayed by the human eye:

$$B_{x1} = \alpha_1 B_T \quad B_{x2} = \alpha_2 B_T \quad B_{x3} = \alpha_3 B_T \tag{15}$$

$$K_1 = \frac{1}{100}\beta \cdot \max\left(\frac{X'(x,y)}{B(x,y)}\right)$$

$$K_2 = K_1\sqrt{B_{x2}}$$

$$K_3 = K_1/B_{x3}. \tag{16}$$

As α_1 is the lower saturation level, it is effective to set this to zero. For α_2 and α_3, it is necessary to determine these experimentally or by using the measure.

By using this information, the image is first broken up into different regions of human visual response based upon B_{xi}, which are the background intensity thresholds between the regions. These different regions are characterized by the minimum difference between two pixel intensities for the HVS to register a difference. Next, these three regions are thresholded by the minimum gradient required for a human observer to notice a change K_i, removing these pixels which do not constitute a noticeable change and placing them in a fourth image. These four segmented images can be arrived at as follows:

$$\begin{aligned}
&\mathrm{Im1} = X(x,y) \\
&\qquad B_{x2} \geq B(x,y) \geq B_{x1} \& \frac{X'(x,y)}{\sqrt{B(x,y)}} \geq K_2 \\
&\mathrm{Im2} = X(x,y) \\
&\qquad \text{such that} \quad B_{x3} \geq B(x,y) \geq B_{x2} \& \frac{X'(x,y)}{B(x,y)} \geq K_1 \\
&\mathrm{Im3} = X(x,y) \\
&\qquad B(x,y) > B_{x3} \& \frac{X'(x,y)}{B(x,y)^2} \geq K_3 \\
&\mathrm{Im4} = X(x,y) \qquad \text{All Remaining Pixels.}
\end{aligned} \tag{17}$$

For practical purposes, it is effective to combine the saturation region and the fourth image. Experimental results show that this does not produce noticeable changes in the output image and has the benefit of reducing the computation time and simplifying the process. This is shown in Figs. 5 and 6, where we show the method using all four regions and the simplified three-region method, showing that they are effectively the same. These three segmented images are obtained using the following formula:

$$\begin{aligned}
&\mathrm{Im1} = X(x,y) \\
&\qquad B_{x2} \geq B(x,y) \geq B_{x1} \& \frac{X'(x,y)}{\sqrt{B(x,y)}} \geq K_2 \\
&\mathrm{Im2} = X(x,y) \\
&\qquad \text{such that} \quad B_{x3} \geq B(x,y) \geq B_{x2} \& \frac{X'(x,y)}{B(x,y)} \geq K_1 \\
&\mathrm{Im3} = X(x,y) \qquad \text{All Remaining Pixels.}
\end{aligned} \tag{18}$$

These three images are then enhanced separately and recombined to form the enhanced image.

Figs. 5 and 6 show the effects of merging the saturation region and the low-contrast region. Fig. 5 shows the actual segmentation results, and Fig. 6 shows the enhanced images. The original cave image is shown in Fig. 6(a), and the enhanced images are shown in Fig. 6(b) and (c). The image in Fig. 6(b) uses three segments, as outlined earlier, and the image in Fig. 6(c) uses all four segments. As shown, the two enhanced images are very similar, with the image using four segments, achieving a slightly better color constancy, particularly among the stalactites along the top of the image. As the two images are very similar, we conclude that three segments are sufficient for the general case. While there may be some cases where four or more segments will achieve significantly better results, for simplicity and time, we use three segments.

Common image enhancement methods include contrast stretching and histogram modeling. These are global algorithms, meaning that they apply the same transform to every

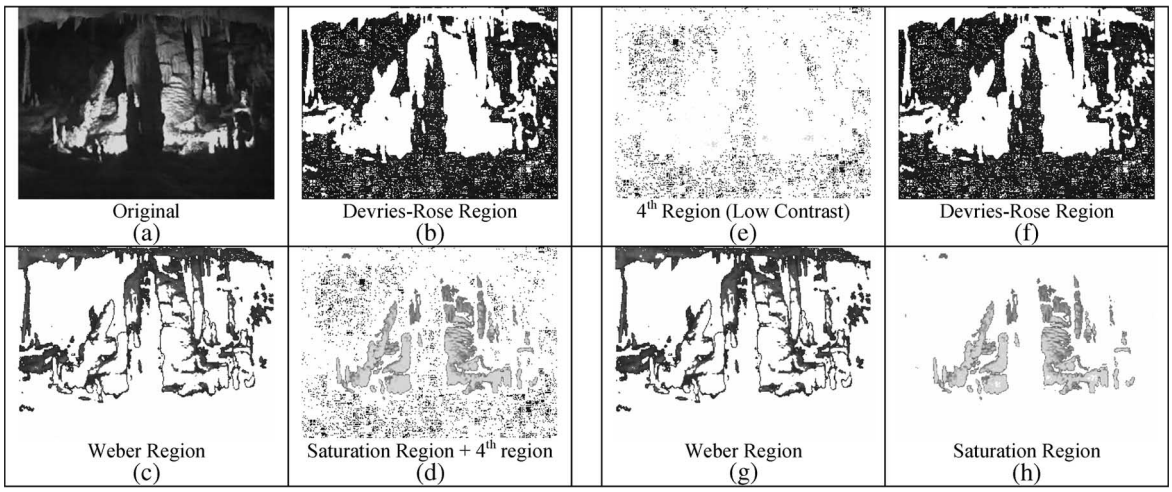

Fig. 5. Demonstration of the HVS-based image enhancement model using three regions versus four regions. The original image (a) is segmented into three subimages (b)–(d), combining the low-contrast fourth region with the saturation region for simplicity. (e)-(f) is the method using all four regions.

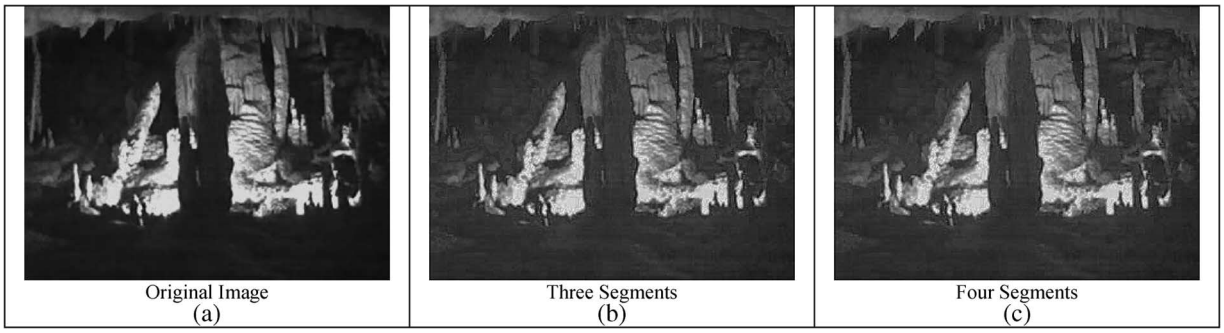

Fig. 6. Determining the best number of segments. (a) Original cave image and the enhanced images using HVS Case 3 with (b) three segments and (c) four segments. This shows that there is no significant difference between using three and four segments.

pixel in the image in the same way, regardless of local image information. However, in many cases, it is necessary to adapt the enhancement within differing regions of the image [12]. This HVS-based algorithm presented can be used for edge detection by keeping the gradient information for only the pixels in the first three segmented regions [33]. However, it can also be modified for use with multihistogram equalization.

A. HVS-Based Multihistogram Equalization

Histogram equalization is a specific case of histogram modeling in which a uniform distribution is forced on an input image. Histogram equalization has been used to correct for uniform brightness issues; however, it also has issues such as changing the overall brightness of an image and adding artifacts. To address this, histogram equalization has been modified to bihistogram equalization, which splits an image into two segments based on a threshold and equalizes the two separately [57]. This is done to maintain the original brightness of the image and reduce artifacts while producing a more visually appealing image. Many methods have been proposed to select this threshold [57], [58], [60], and the extension to generalized histogram modeling [61] and multihistogram equalization [59] have been proposed. Dualistic subimage histogram equalization (DSHE) selects the threshold to have an equal number of pixels both above and below the threshold, in an attempt to maximize entropy [58]. Histogram modeling attempts to force a desired histogram on an image instead of converting to a flat histogram [61]. Recursive mean-separate histogram equalization (RMSHE) is a multihistogram equalization method which thresholds an image histogram based on the mean recursively, arriving at either two, four, or eight subimages which are equalized separately [59].

Fig. 7 shows the basic multihistogram equalization approach; DSHE [58] using two subimages and RMSHE [59] using four subimages. The basic method for RMSHE is shown in Fig. 7, demonstrating the thresholding step and the result of the separate equalizations. For DSHE, one simply skips the second threshold step, equalizing the images in the second column. While this thresholding method achieves better results than standard histogram equalization, it can be improved. The threshold value used in Fig. 7 results in an image containing only the darkest parts of the image and another image which contains a visually pleasing portion as well as an over-illuminated portion. Additionally, the regions do not always correspond to the physical regions present. This causes the unnatural appearance mentioned in [57], which is common to histogram equalization methods. The segmented regions still do not always correspond to the actual physical regions because the thresholding is performed directly on the pixel intensities.

In this paper, we propose a multihistogram equalization method in which models of the HVS are used to segment the

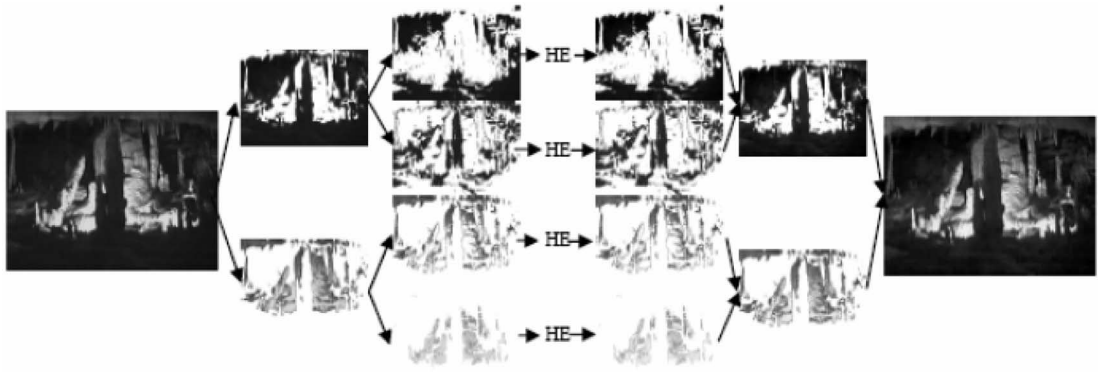

Fig. 7. Demonstration of multihistogram equalization methods from the literature, showing RMSHE. If only the first threshold step was performed, this would be DSHE. Because these methods threshold directly the pixel intensity values, this segmentation method can be improved.

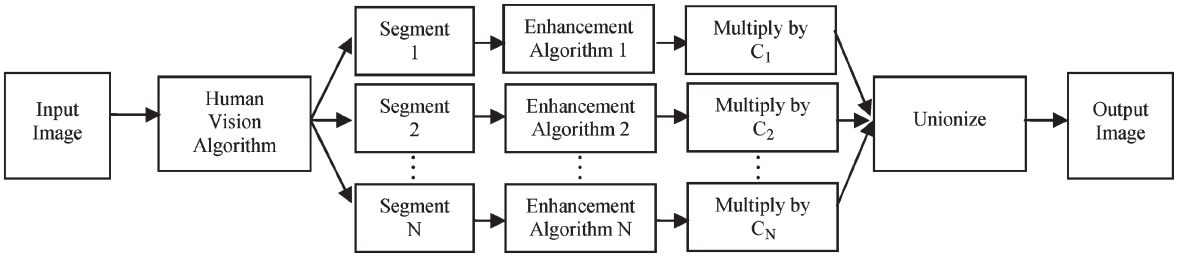

Fig. 8. Flow chart for human-vision-based image enhancement for $N = 3$ or 4 segments.

image, as shown in the block diagram in Fig. 8. This allows for a more consistent segmentation and output results which are more visually pleasing to a human observer. This method is then improved through the use of bihistogram equalization on each segment, increasing the segmentation from three to six segments, improving performance accordingly. In this diagram, $C_1, C_2, \ldots, C_N$ are used to ensure a visually consistent output image.

B. HVS-Based Image Enhancement

As the use of an HVS-based segmentation method improves the performance of multihistogram equalization, it is natural to ask if such a solution could be applied to other enhancement problems as well. We find that it is possible to extend the HVS-based method to other global enhancement algorithms to find a general case of HVS-based image enhancement. For this method, we utilize the segmentation shown in Fig. 8, but extend it to use any global enhancement algorithms. This allows for more adaptable image enhancement which is better able to address local features of an image using less complex global algorithms, relying on models of the HVS to ensure visually appealing output.

Fig. 8 shows the use of this algorithm, using the segmentation demonstrated earlier. First, the image is split into three subimages or segments based upon the graph in Fig. 5. Notice how the subimages individually have similar characteristics, allowing for a much simpler enhancement. Next, each image is enhanced separately. Finally, the three images are scaled by a constant to ensure a consistent appearance and recombined to form the output image.

C. Selection of Parameters Using the Measure

Selection of the l and q constants can be performed using the logarithmic AMEE measure. This is done in the same manner as selecting the α constants, as shown in Fig. 9. The absolute maximum of the EMEE graph occurred at $l = 0.9$ and $q = 1.4$. After a number of possible values from the EMEE graph were tested, it was found that the values resulting in this absolute maximum are the best.

Selection of the α constants, while slightly different for different images, is efficiently done using the logarithmic AMEE measure. This is shown in Fig. 9. Fig. 9(a) and (b) shows the original image and the image processed with global histogram equalization, Fig. 9(c) shows the output of HVS-based multihistogram equalization, and Fig. 9(d) shows the graph used to select α_2 and α_3.

The graph in Fig. 9(d) shows a number of "ridges" along constant values of α_2 and α_3. Selection of these parameters is then as simple as locating the intersection between these ridges in an acceptable place. As several of the ridges would intersect in places where $\alpha_3 < \alpha_2$, this greatly reduces the number of false positives. The answer then lies at the most prominent local maximum; in this case, $\alpha_2 = 0.12$, and $\alpha_3 = 0.63$. These are the parameters used for the image in Fig. 9(c). This image does not lose any of the information from the illuminated side of the image, as is the case with global histogram equalization.

V. Enhancement Algorithms

In this section, we present novel enhancement algorithms used in conjunction with HVS-based image enhancement. We

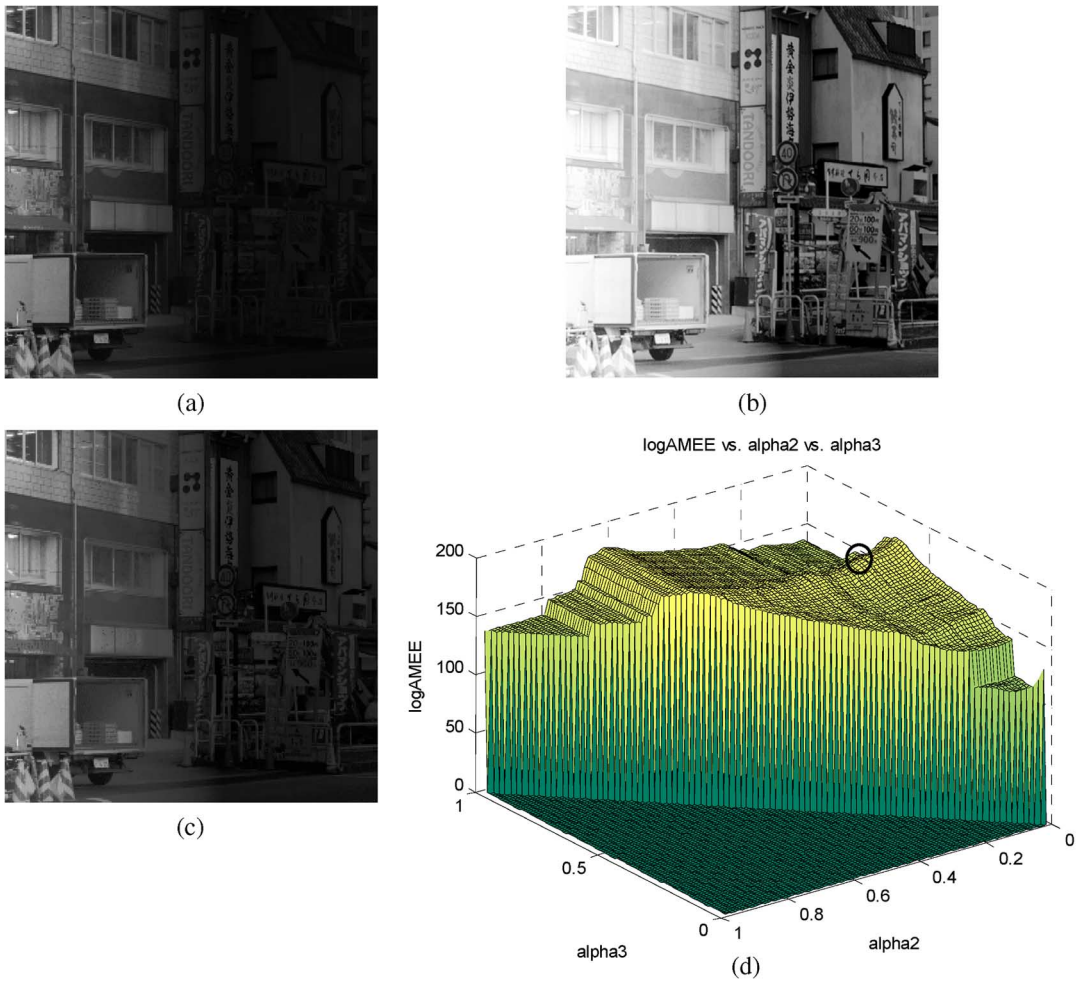

Fig. 9. Using the logarithmic AMEE contrast measure to select α_2 and α_3. (a) Original image. (b) Original image enhanced with global histogram equalization. (c) Original image enhanced with HVS-based multihistogram equalization. (d) Logarithmic AMEE graph used to select parameters. The values are taken from the largest local maxima, occurring at $\alpha_2 = 0.12$ and (circled) $\alpha_3 = 0.63$.

present the EPCE algorithm and the LAW image enhancement algorithm. We also summarize the use of these algorithms with the HVS model.

A. Edge-Preserving Contrast Enhancement (EPCE)

It is well known that human eyes have a much larger dynamic range than current imaging and display devices. Traditional methods for image enhancement, such as gamma adjustment, logarithmic compression, histogram equalization, and level or curve-type methods, are generally limited because they process images globally. To solve this, more advanced methods have been introduced based on better understanding of the HVS, which are more capable of handling scenes with high dynamic ranges. Many of these methods make use of spatially dependent processing methods, where each pixel is determined by both local and global image information [62].

EPCE is a contrast enhancement algorithm which is designed to preserve edges while improving contrast on a local scale by combining the output of an edge-detection algorithm with the original spatial image information. This achieves a more robust enhancement algorithm that is tunable to perform edge detection or enhancement [34]. This enhancement algorithm can work with any suitable edge-detection algorithm. It uses preprocessing steps to standardize image brightness and several postprocessing steps to enhance the edges contained.

The first part of this algorithm is performed on each image pixel and is based on the local mean at each pixel, using the following formula:

$$I(x,y) = \frac{2}{1 + e^{-2\tau(x,y)/\lambda(x,y)}} - 1 \tag{19}$$

where $I(x,y)$ is the output image, $\tau(x,y)$ is either the V component of the image in HVS color space or the gray scale image, and λ is the local statistic of the image used to adjust the transfer function to the local mean. Finally, λ is

$$\lambda(x,y) = C + (M - C)\left(\frac{\mu(x,y)}{M(Qx+N)}\right) \tag{20}$$

where C is a user-selected enhancement parameter, with effective range $0 = C < 256$, M is the maximum value of the range, and $\mu(x,y)$ is the local mean of the image. In the succeeding discussion, we select the optimal values for C using the measures (14) and (15).

Fig. 10. Selection of parameters for the EPCE algorithm using the LogAMEE measure. (a) Image processed with $\alpha = 1$ and $\gamma = 1$. (b) Image processed with $\alpha = 0.2$ and $\gamma = 0.6$, which are taken from the only local maxima in the LogAMEE graph in (c).

After this, a second step is performed to enhance the contrast. This is performed by first applying a high-pass filter on the image, then enhancing this image. We will call this I_{EN}. For this step, any common enhancement algorithm can be used, such as alpha rooting or logarithmic enhancement [7]. Next, apply edge detection, resulting in the image that we will call I_{ED}. Finally, the following formula gives the output-enhanced image:

$$I_{F,\mathrm{EN}} = A\left(I(x,y) + I_{\mathrm{ED}}(x,y)^{\gamma} \times I_{\mathrm{EN}}(x,y)^{\alpha}\right) \qquad (21)$$

where $I_{F,\mathrm{EN}}$ is the output image and A, α, and γ are user-defined operating parameters.

As this enhancement algorithm has a number of parameters which must be selected, we next demonstrate the selection of parameters using the logarithmic AMEE measure. Selection of M and C can be done simply and quickly by a human; however, selecting α and γ is a more time-consuming task. This process is shown in Fig. 10. For this image, $M = 260$ and $C = 50$. The image is shown in Fig. 10(a), processed with $\alpha = 1$ and $\gamma = 1$. Fig. 10(b) shows the enhanced image using $\alpha = 0.2$ and $\gamma = 0.6$, which are selected from the logarithmic AMEE graph in Fig. 10(c). These values are those from the only peak in the graph and result in a much more visually pleasing enhanced image. This image has greatly improved contrast and sharpness.

B. Logarithm and AME-Based Weighted Passband (LAW)

This algorithm capitalizes on the AME measure to enhance details of an image while removing noise and is further improved by using the PLIP model. The LAW algorithm has no parameters; instead, it uses the AME measure to give each result a score and averages the results based on the results from this measure. It employs a multipass technique. For each pass, the image is first decomposed into two separate images. The first image is processed with a low-pass filter. The second image consists of the difference between the original and low-pass images. These two images are then weighted and added back together to get the result for that passband [10]. This algorithm is further improved by parameterization using the PLIP model. This method uses the following expression:

$$f'(i,j) = C \cdot (\gamma \otimes a(i,j) \oplus n \otimes [f(i,j) \Theta a(i,j)]) \qquad (22)$$

where $f'(i,j)$ is the output gray tone function, $f(i,j)$ is the input gray tone function, $a(i,j)$ is the low-pass version of the image, and γ and n are user-defined operating constants. This is performed multiple times for different passbands on the low-pass filter, and the final image is the weighted sum of these images, using the AME for the weights.

C. HVS-Based Image Enhancement

HVS-based image enhancement, as stated previously, segments an image into three regions based on local image properties and allows these images to be enhanced separately. In this section, the use of the HVS model with global image enhancement algorithms is demonstrated. Fig. 8 from Section IV shows a block diagram of this process, and Table II shows several possible combinations for use with this method.

VI. Computational Analysis

In this section, we present a computational analysis comparing the HVS algorithm to current state-of-the-art algorithms. Earlier work in tone reproduction for high contrast images has included tone reproduction methods that manipulate the pixel distributions to match display brightness with real-world sensations [63]. Good results have also been achieved using learning-based tone reproduction curves (TRCs) and a fast implementation thereof [64], [65].

Outstanding work has been done in these areas by Tumblin and Turk [55] using an LCIS method as the basis for image enhancement. Excellent results have also been achieved by Qiu and Duan [56] using a binary-tree-based TRC method. We briefly present these two methods and present a comparison using these two algorithms as a standard for the HVS algorithm.

It would be desirable to compare implementations of these algorithms to establish actual benchmark metrics for HVS. However, explicit implementation details of each algorithm are unavailable, so any implementation would be our interpretation; thus, the comparison could not be presented with confidence. In lieu of this, we provide a computational analysis on our interpretation of each algorithm, as presented in the literature.

Tumblin and Turk [55] utilize an LCIS, which is a partial differential equation inspired by anisotropic diffusion. The

TABLE II
COMBINATIONS FOR USE WITH HVS-BASED IMAGE ENHANCEMENT

	Segment 1	Segment 2	Segment 3
Case 1	Histogram Equalization	Histogram Equalization	Histogram Equalization
Case 2	LAW	LAW	LAW
Case 3	LAW	LAW	Histogram Equalization
Case 4	EPCE	LAW	Histogram Equalization
Case 5	Alpha Rooting	Alpha Rooting	Alpha Rooting
Case 6	Histogram Equalization	EPCE	Histogram Equalization
Case 7	EPCE	EPCE	Alpha Rooting

(a) (b) (c)

Fig. 11. Sample results comparing LCIS to HVS method. (a) Original school. (b) LCIS-enhanced school. (c) HVS-enhanced school.

algorithm first uses the LCIS to arrive at a smoothed image that maintains the image edges and progressively adds the details to this image in much the same way as an artist develops a scene. An example of the LCIS method is shown in Fig. 11.

As this method is dependent on the desired number of timescales used, time and computational complexity can vary depending on the image and application. However, in general, this algorithm calculates 13 partial derivatives, 2 motive forces, 2 edge maps, 2 leakfix multipliers, 2 conductances, 2 fluxes, and 1 new pixel for every pixel and for every timescale [55]. HVS-based image enhancement, on the other hand, calculates background illumination and gradient once for each pixel, calculates seven constants, and performs three enhancement algorithms of choice.

Qiu and Duan [56] utilize an optimal TRC operator for enhancement, manipulating pixel distributions based upon a binary tree. This method is based upon a cost function, comparing traditional histogram equalization with linear scale mapping to achieve the optimal threshold, resulting in an output image with the best aspects of both traditional enhancement algorithms.

As this is a binary-tree method for which every gray level must be tested at every step, it can be shown that this method is of the order $O(n \log n)$. For every iteration, E_b must be calculated for every gray level, and for every iteration, the number of remaining thresholds to be assigned is halved. Assuming 256 gray levels, E_b utilizes 260 additions, 7 multiplications, and 2 divisions and calculates the histogram [56].

The HVS-based enhancement method, on the other hand, is run once for an image and is of the order $O(n)$. It calculates gradient, illumination, and thresholds for every pixel, as well as a small number of global thresholds. The gradient uses two PLIP subtractions; the background illumination uses ten PLIP additions and four PLIP scalar multiplications, and the final thresholding operation uses two PLIP gray multiplications and one square root. This results in a total of 38 additions, 22 multiplications, 22 divisions, 8 exponentiations, 4 logarithms, and 1 square root, which must be calculated for every pixel. The global constant calculations utilize one PLIP minus, six PLIP scalar multiplications, one PLIP gray multiplication, and one square root. This results in 17 additions, 10 multiplications, 10 divisions, 8 exponentiations, 2 logarithms, and 1 square root, which must be calculated once for each image.

VII. COMPUTER SIMULATIONS

In this section, we use the proposed measure to show the results of computer simulations with the presented image enhancement algorithms. We compare it with the results of the Retinex algorithm and histogram equalization, since these are comparable fully automated image enhancement algorithms. For the basis of comparison, we use the logarithmic AME to assess the enhancement quality.

Fig. 12 shows the results for all images, and Tables III and IV compare the performances subjectively and objectively. The original images in Fig. 12 are comprised of a collection of images that are representative of many common image enhancement problems. The first row of images (a)–(d) shows professionally captured images with regions of illumination, which is a traditionally difficult problem to solve. The first two images in the second row (e)–(f) are camera phone images, taken with a Motorola RAZR V3 0.3-megapixel camera phone. These also show regions of illumination in addition to a lower quality digitization and a lower resolution. The remaining images in the second row (g)–(h) are professionally captured aerial images and are common test images. The first two images in the third row (i)–(j) are professionally captured images with textures and shadows, and the last two images in the third row (k)–(l) are commonly used test images.

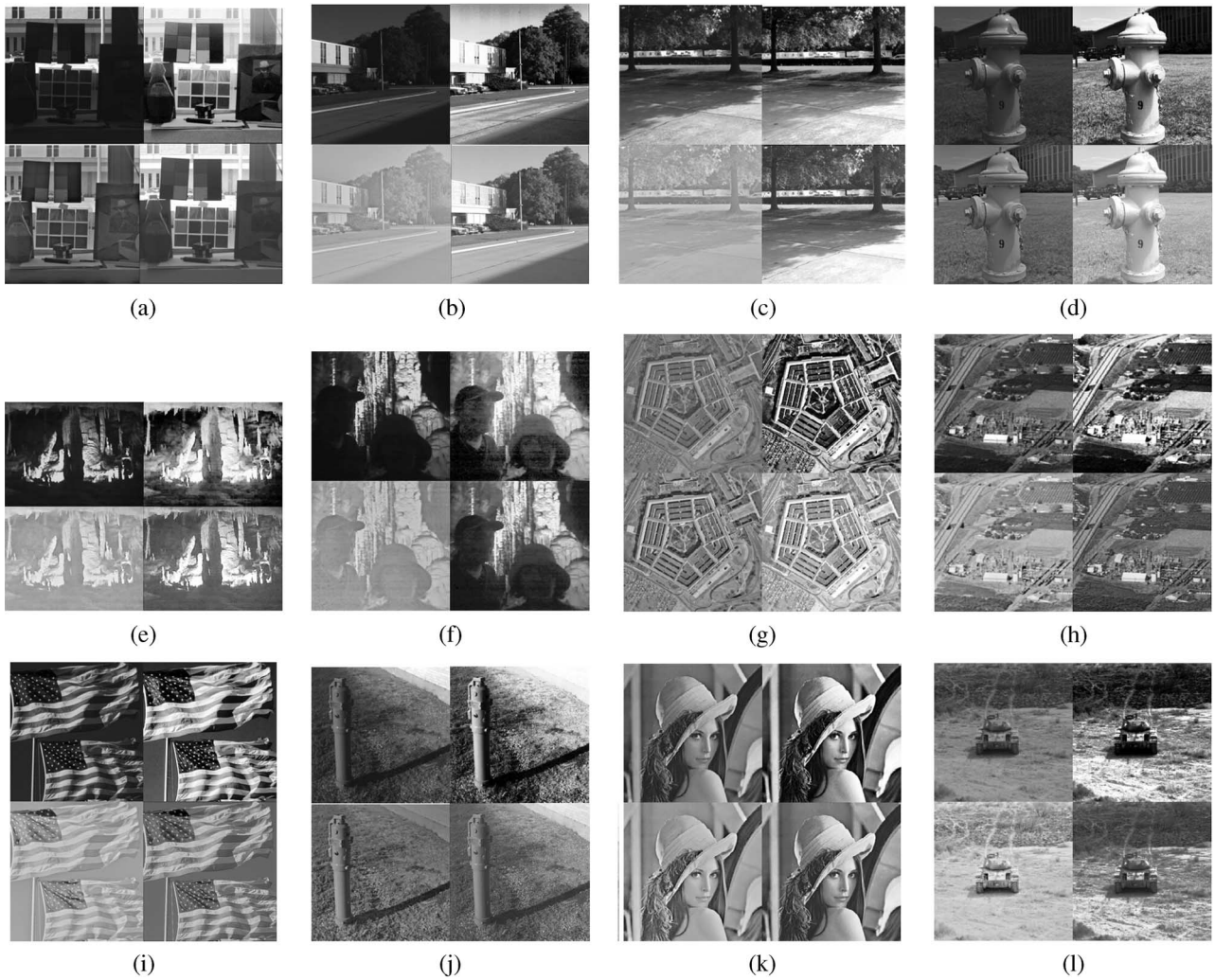

Fig. 12. HVS versus Retinex results for all images. (Top left) Original image. (Top right) Histogram equalization. (Bottom left) Retinex. (Bottom right) HVS-based image enhancement.

TABLE III
SUBJECTIVE RESULTS

	Histogram Equalization	Retinex	HVS Method
Desk	**	**	***
School	**	*	***
Shadows	**	*	***
Hydrant	*	**	***
Cave	**	*	***
Faces	**	*	***
Pentagon	*	**	***
Plant	**	*	***
Flags	**	**	***
Hydrant2	*	**	***
Lena	*	**	***
Tank	**	*	***
* = Fair, ** = Good, *** = Best			

TABLE IV
OBJECTIVE RESULTS USING LOGAME MEASURE

	Original logAME	Histogram Equalization	Retinex	HVS case 3	HVS case 4
Desk	44.5499	46.9275	47.8846	92.9685	510.9374
School	44.2793	49.1396	24.2388	59.8965	272.1211
Shadows	70.0900	68.9807	36.1967	142.0852	137.9644
Hydrant	63.3895	56.4526	65.7128	65.255	66.4489
Cave	20.9560	21.5783	12.7700	67.0823	66.7669
Faces	52.0727	48.1594	29.4644	66.8274	62.3067
Pentagon	15.7386	12.2778	16.6089	17.0522	17.8118
Plant	16.9992	15.3536	14.6112	17.0704	17.2489
Flags	44.6210	42.7614	31.6806	45.5378	45.4235
Hydrant2	64.8002	55.2555	64.2423	68.7349	71.3116
Lena	12.0810	11.2272	11.0692	15.1728	13.3927
Tank	9.4790	9.6103	8.3632	9.8809	19.1409

To assess the performance of the enhancement methods, several human interpreters were asked to arrange the images from best to worst. The average performance of each is shown in Table III. For some results, perceived brightness may have skewed results toward global histogram equalization. This is because histogram equalization always increases contrast, sometimes unnaturally. The results of this subjective evaluation show that, for every image, the HVS method outperforms the other two methods. However, an objective criterion is also necessary.

The logarithmic AME values are shown in Table IV. These results show large increases in the LogAME values for some of the most difficult cases. For simpler cases, these values show that the HVS method matches or slightly outperforms the other methods. The strong performances of two separate HVS cases on all images demonstrate the robustness of the HVS method.

Also, cases like the desk image, where there is a large jump from one case to the other, demonstrate the potential of this method when enhancement algorithms are carefully selected to match the individual subimages.

In summary, the presented HVS-based image enhancement methods outperform the other enhancement methods on the basis of subjective and objective analyses. In particular, for the difficult cases of varying scene illumination, the proposed method shows great improvement over the other methods used for comparison. The consistent performance on all images is also seen, demonstrating the robustness and performance of the HVS method.

VIII. Conclusion

In this paper, a new HVS-based image enhancement method was presented. A number of enhancement algorithms, which can be used in conjunction with the HVS method, were also presented. A novel algorithm (EPCE) was presented to improve local contrast while maintaining the edge information. We introduced HVS-based multihistogram equalization and the extension to the general case of HVS-based image enhancement. The HVS method segments an image based upon background illumination to achieve results which cannot be achieved using global methods. This method allows for correction of nonuniform illumination, shadows, and other traditionally difficult issues. A comparison was presented showing that the proposed method outperforms other leading methods, both subjectively and objectively.

A novel measure of image enhancement, called the logarithmic AMEE, was also presented. This measure combines previously used measures of image enhancement with the PLIP model to obtain a better measure of image enhancement. A comparison between the proposed measure and previously used measures shows that the proposed measure is able to better select parameters. This can help in removing the human element from image enhancement systems, allowing for more consistent results and opening the possibility for automating more complex image enhancement methods. Future applications of the HVS model could also include noise removal. Some noise models, such as salt and pepper, affect only one or two segments without affecting all segments. As such, it would be effective to use the HVS model to separate out the noisy portion and obtain a simpler noise removal problem.

References

[1] M. W. Powell, S. Sarkar, D. B. Goldgof, and K. Ivanov, "A methodology for extracting objective color from images," *IEEE Trans. Syst., Man, Cybern. B, Cybern.*, vol. 34, no. 5, pp. 1964–1978, Oct. 2004.

[2] Z. Tianxu, P. Jiaxiong, and L. Zongjie, "An adaptive image segmentation method with visual nonlinearity characteristics," *IEEE Trans. Syst., Man, Cybern. B, Cybern.*, vol. 26, no. 4, pp. 619–627, Aug. 1996.

[3] B. Bhanu, J. Peng, T. Huang, and B. Draper, "Introduction to the special issue on learning in computer vision and pattern recognition," *IEEE Trans. Syst., Man, Cybern. B, Cybern.*, vol. 35, no. 3, pp. 391–396, Jun. 2005.

[4] P. Csákány and A. M. Wallace, "Representation and classification of 3-D objects," *IEEE Trans. Syst., Man, Cybern. B, Cybern.*, vol. 33, no. 4, pp. 638–647, Aug. 2003.

[5] M. Zhang, L. O. Hall, and D. B. Goldgof, "A generic knowledge-guided image segmentation and labeling system using fuzzy clustering algorithms," *IEEE Trans. Syst., Man, Cybern. B, Cybern.*, vol. 32, no. 5, pp. 571–582, Oct. 2002.

[6] A. Y. Mülayim, U. Yilmaz, and V. Atalay, "Silhouette-based 3-D model reconstruction from multiple images," *IEEE Trans. Syst., Man, Cybern. B, Cybern.*, vol. 33, no. 4, pp. 582–591, Aug. 2003.

[7] G. Guidi, J. A. Beraldin, S. Ciofi, and C. Atzeni, "Fusion of range camera and photogrammetry: A systematic procedure for improving 3-D models metric accuracy," *IEEE Trans. Syst., Man, Cybern. B, Cybern.*, vol. 33, no. 4, pp. 667–676, Aug. 2003.

[8] S. Y. Chen and Y. F. Li, "Vision sensor planning for 3-D model acquisition," *IEEE Trans. Syst., Man, Cybern. B, Cybern.*, vol. 35, no. 5, pp. 894–904, Oct. 2005.

[9] C. Munteanu and A. Rosa, "Gray-scale image enhancement as an automatic process driven by evolution," *IEEE Trans. Syst., Man, Cybern. B, Cybern.*, vol. 34, no. 2, pp. 1292–1298, Apr. 2004.

[10] G. Deng, L. W. Cahill, and G. R. Tobin, "The study of logarithmic image processing model and its applications to image enhancement," *IEEE Trans. Image Process.*, vol. 4, no. 4, pp. 506–512, Apr. 1995.

[11] W. K. Pratt, *Digital Image Processing*. New York: Wiley, 2000.

[12] R. C. Gonzales and R. E. Woods, *Digital Image Processing*. Reading, MA: Addison-Wesley, 1987.

[13] M. Jourlin and J. C. Pinoli, "Logarithmic image processing: The mathematical and physical framework for the representation and processing of transmitted images," *Adv. Imag. Electron Phys.*, vol. 115, pp. 129–196, 2001.

[14] T. G. Stockham, Jr., "Image processing in the context of a visual model," *Proc. IEEE*, vol. 60, no. 7, pp. 828–842, Jul. 1972.

[15] D. J. Granrath, "The role of human visual models in image processing," *Proc. IEEE*, vol. 69, no. 5, pp. 552–561, May 1981.

[16] S. Agaian, B. Silver, and K. Panetta, "Transform coefficient histogram based image enhancement algorithms using contrast entropy," *IEEE Trans. Image Process.*, vol. 16, no. 3, pp. 741–758, Mar. 2007.

[17] A. Polesel, G. Ramponi, and V. J. Mathews, "Image enhancement via adaptive unsharp masking," *IEEE Trans. Image Process.*, vol. 9, no. 3, pp. 505–510, Mar. 2000.

[18] H. D. Cheng and H. Xu, "A novel fuzzy logic approach to contrast enhancement," *Pattern Recognit.*, vol. 33, no. 5, pp. 809–819, May 2000.

[19] P. Natendra and R. C. Rithch, "Real-time adaptive contrast enhancement," *IEEE Trans. Pattern Anal. Mach. Intell.*, vol. PAMI-3, no. 6, pp. 655–661, Nov. 1981.

[20] R. H. Sherrier and G. A. Johnson, "Regionally adaptive histogram equalization of the chest," *IEEE Trans. Med. Imag.*, vol. MI-6, no. 1, pp. 1–7, Mar. 1987.

[21] A. Beghdadi and A. L. Negrate, "Contrast enhancement technique based on local detection of edges," *Comput. Vis. Graph. Image Process.*, vol. 46, no. 2, pp. 162–274, May 1989.

[22] J. K. Kim, J. M. Park, K. S. Song, and H. W. Park, "Adaptive mammographic image enhancement using first derivative and local statistics," *IEEE Trans. Med. Imag.*, vol. 16, no. 5, pp. 495–502, Oct. 1997.

[23] W. M. Morrow, R. B. Paranjape, R. M. Rangayyan, and J. E. L. Desautels, "Region-based contrast enhancement of mammograms," *IEEE Trans. Med. Imag.*, vol. 11, no. 3, pp. 392–406, Sep. 1992.

[24] J. A. Saghri, P. S. Cheatham, and H. Habibi, "Image quality measure based on a human visual system model," *Opt. Eng.*, vol. 28, no. 7, pp. 813–818, Jul. 1989.

[25] G. X. Ritter and J. N. Wilson, *Handbook of Computer Vision Algorithms in Image Algebra*. Boca Raton, FL: CRC, 1996.

[26] J. Tang, E. Peli, and S. Acton, "Image enhancement using a contrast measure in the compressed domain," *IEEE Signal Process. Lett.*, vol. 10, no. 10, pp. 289–292, Oct. 2003.

[27] A. A. Michelson, *Studies in Optics*. Chicago, IL: Univ. Chicago Press, 1927.

[28] A. Khellaf, A. Beghdadi, and H. Dupoiset, "Entropic contrast enhancement," *IEEE Trans. Med. Imag.*, vol. 10, no. 4, pp. 589–592, Dec. 1991.

[29] S. S. Agaian, K. Panetta, and A. Grigoryan, "Transform-based image enhancement algorithms with performance measure," *IEEE Trans. Image Process.*, vol. 10, no. 3, pp. 367–382, Mar. 2001.

[30] S. S. Agaian, "Visual morphology," in *Proc. SPIE, Nonlinear Image Process. X*, San Jose, CA, Mar. 1999, vol. 3646, pp. 139–150.

[31] S. S. Agaian, K. Panetta, and A. M. Grigoryan, "A new measure of image enhancement," presented at the *IASTED Int. Conf. Signal Processing Communication*, Marbella, Spain, 2000.

[32] E. Wharton, S. Agaian, and K. Panetta, "Comparative study of logarithmic enhancement algorithms with performance measure," in *Proc. SPIE Electron. Imag.*, San Jose, CA, Jan. 17, 2006, pp. 606 412–606 413.

[33] M. K. Kundu and S. K. Pal, "Thresholding for edge detection using human psychovisual phenomena," *Pattern Recognit. Lett.*, vol. 4, no. 6, pp. 433–441, Dec. 1986.

[34] E. Wharton, S. Agaian, and K. Panetta, "A logarithmic measure of image enhancement," in *Proc. SPIE, Defense Security Symp.*, Orlando, FL, Apr. 20, 2006, p. 62 500P.
[35] J. Tang, J. Kim, and E. Peli, "Image enhancement in the JPEG domain for people with vision impairment," *IEEE Trans. Biomed. Eng.*, vol. 51, no. 11, pp. 2013–2023, Nov. 2004.
[36] D. J. Jobson, Z. Rahman, and G. A. Woodell, "Properties and performance of a center/surround Retinex," *IEEE Trans. Image Process.*, vol. 6, no. 3, pp. 451–462, Mar. 1997.
[37] J. H. McClellan, "Artifacts in alpha-rooting of images," in *Proc. IEEE Int. Conf. Acoust., Speech, Signal Process.*, Apr. 1980, pp. 449–452.
[38] R. Kogan, S. Agaian, and K. A. Panetta, "Visualization using rational morphology and magnitude reduction II," in *Proc. SPIE's Symp. Electron. Imag. Sci. Technol.*, Orlando, FL, Apr. 1998, vol. 3387, pp. 301–312.
[39] R. Kogan, S. S. Agaian, and K. Panetta, "Visualization using rational morphology and zonal magnitude-reduction," *Proc. SPIE*, vol. 3304, pp. 153–163, 1998.
[40] S. Aghagolzadeh and O. K. Ersoy, "Transform image enhancement," *Opt. Eng.*, vol. 31, no. 3, pp. 614–626, Mar. 1992.
[41] R. A. Nobakht and S. A. Rajala, "An image coding technique using a human visual system model and image analysis criteria," in *Proc. IEEE Int. Conf. Acoust., Speech, Signal Process.*, Apr. 1987, vol. 12, pp. 1358–1361.
[42] J. Dušek and K. Roubík, "Testing of new models of the human visual system for image quality evaluation," in *Proc. IEEE 7th Int. Symp. Signal Process. Appl.*, Jul. 2003, vol. 2, pp. 621–622.
[43] K. Panetta, E. Wharton, and S. Agaian, "Parameterization of logarithmic image processing models," *IEEE Trans. Syst., Man, Cybern. A, Syst., Humans*, Jan. 2007, submitted for publication.
[44] D. Marr, *A Computational Investigation Into the Human Representation and Processing of Visual Information*. San Francisco, CA: Freeman, 1982.
[45] D. G. Myers, *Digital Signal Processing: Efficient Convolution and Fourier Transform Techniques*. Upper Saddle River, NJ: Prentice-Hall, 1990.
[46] J. C. Brailean, B. J. Sullivan, C. T. Chen, and M. L. Giger, "Evaluating the EM algorithm for image processing using a human visual fidelity criterion," in *Proc. Int. Conf. Acoust., Speech, Signal Process.*, 1991, pp. 2957–2960.
[47] J. C. Brailean *et al.*, "Application of the EM algorithm to radiographic images," *Med. Phys.*, vol. 19, no. 5, pp. 1175–1182, Sep. 1992.
[48] M. Jourlin, J. C. Pinoli, and R. Zeboudj, "Contrast definition and contour detection for logarithmic images," *J. Microsc.*, vol. 156, no. 1, pp. 33–40, Oct. 1989.
[49] H. Konik, B. Laget, and M. Calonnier, "Segmentation d'images par utilisation de pyramides à bases locales," *Trait. Signal*, vol. 10, no. 4, pp. 283–295, 1993.
[50] J. C. Pinoli, "Metrics, scalar product and correlation adapted to logarithmic images," *Acta Stereol.*, vol. 11, no. 2, pp. 157–168, Dec. 1992.
[51] C. Mota and J. Gomes, "Curvature operators in geometric image processing," in *Proc. IEEE Braz. Symp. Comput. Graph. Image Process.*, 1999, pp. 223–230.
[52] G. Buchsbaum, "An analytical derivation of visual nonlinearity," *IEEE Trans. Biomed. Eng.*, vol. BME-27, no. 5, pp. 237–242, May 1980.
[53] J. Rovamo, J. Mustonen, and R. Nasanen, "Modelling contrast sensitivity as a function of retinal illuminance and grating area," *Vis. Res.*, vol. 34, no. 10, pp. 1301–1314, May 1994.
[54] A. K. Jain, *Fundamentals of Digital Image Processing*. Upper Saddle River, NJ: Prentice-Hall, 1989.
[55] J. Tumblin and G. Turk, "LCIS: A boundary hierarchy for detail-preserving contrast reduction," in *Proc. ACM 26th Conf. Comput. Graph. Interactive Tech.*, 1999, pp. 83–90.
[56] G. Qiu and J. Duan, "An optimal tone reproduction curve operator for the display of high dynamic range images," in *Proc. IEEE Int. Symp. Circuits Syst.*, 2005, vol. 6, pp. 6276–6279.
[57] Y.-T. Kim, "Contrast enhancement using brightness preserving bi-histogram equalization," *IEEE Trans. Consum. Electron.*, vol. 43, no. 1, pp. 1–8, Feb. 1997.
[58] Y. Wang, Q. Chen, and B. Zhang, "Image enhancement based on equal area dualistic sub-image histogram equalization method," *IEEE Trans. Consum. Electron.*, vol. 45, no. 1, pp. 68–75, Feb. 1999.
[59] S.-D. Chen and A. R. Ramli, "Contrast enhancement using recursive mean-separate histogram equalization for scalable brightness preservation," *IEEE Trans. Consum. Electron.*, vol. 49, no. 4, pp. 1301–1309, Nov. 2003.
[60] S.-D. Chen and A. R. Ramli, "Minimum mean brightness error bi-histogram equalization in contrast enhancement," *IEEE Trans. Consum. Electron.*, vol. 49, no. 4, pp. 1310–1319, Nov. 2003.
[61] C. Wang and Z. Ye, "Brightness preserving histogram equalization with maximum entropy: A variational perspective," *IEEE Trans. Consum. Electron.*, vol. 51, no. 4, pp. 1326–1334, Nov. 2005.
[62] L. Tao, M. J. Seow, and V. K. Asari, "Nonlinear image enhancement to improve face detection in complex lighting environment," in *Proc. SPIE Electron. Imag.*, 2006, vol. 6064, p. 606 416.
[63] J. Tumblin and H. Rushmeier, "Tone reproduction for realistic images," *IEEE Comput. Graph. Appl.*, vol. 13, no. 6, pp. 42–48, Nov. 1993.
[64] J. Duan, G. Qiu, and G. D. Finlayson, "Learning to display high dynamic range images," in *Proc. IS&T's 2nd Eur. Conf. CGIV*, Aachen, Germany, Apr. 5–8, 2004, pp. 542–547.
[65] J. Duan and G. Qiu, "Fast tone mapping for high dynamic range images," in *Proc. 17th ICPR*, Cambridge, U.K., Aug. 23–26, 2004, pp. 847–850.

Karen A. Panetta (S'84–M'85–SM'95–F'08) received the B.S. degree in computer engineering from Boston University, Boston, MA, and the M.S. and Ph.D. degrees in electrical engineering from Northeastern University, Boston.

She is currently a Consulting Engineer with Tyco Electronics Inc., Lowell, MA. She is also the cofounder of BA Logix, Inc., Quincy, MA, and serves as the company's Chief Research Scientist.

Dr. Panetta is the 2008 IEEE Director of Women in Engineering and is the Editor-in-Chief of the IEEE WOMEN IN ENGINEERING Magazine.

Eric J. Wharton (S'04) received the B.S. degree in electrical engineering from Tufts University, Medford, MA, where he is currently working toward the M.S. degree.

His primary research interests include digital signal and image processing, specifically image enhancement and performance measures.

Mr. Wharton is a member of Eta Kappa Nu and Tau Beta Pi.

Sos S. Agaian (M'98–SM'00) received the M.S. degree (*summa cum laude*) in mathematics and mechanics from Yerevan State University, Yerevan, Armenia, the Ph.D. degree in mathematics and physics and the Doctor of Engineering Sciences (equivalent to the US Doctor of Electrical and Computer Engineering) degree from the Academy of Sciences of the USSR, Moscow, Russia, and the Diploma in computer science (equivalent to the US Ph.D. degree in computer science) from the Supreme Attestation Board of the USSR, Moscow.

He is currently the Peter T. Flawn Distinguished Professor with the College of Engineering, University of Texas at San Antonio, San Antonio, and an Adjunct Professor with the Department of Electrical and Computer Engineering, Tufts University, Medford, MA. He is the author of more than 350 scientific papers and four books and is the holder of 13 patents. He is an Associate Editor for the *Journal of Real-Time Imaging* and the *Journal of Electronic Imaging* and an Editorial Board Member of the *Journal of Pattern Recognition and Image Analysis*. His current research interests include signal/image processing and transmission, multimedia security, digital forensics, vision networks, and mobile imaging and secure communication.

Dr. Agaian is a Fellow of the International Society for Photo-Optical Instrumentations Engineers (SPIE).